






## RESEARCH ARTICLE

# Zwitterionic ring expansion polymerization of *tert*-butyl glycidyl ether with $B(C_6F_5)_3$ towards the generation of cyclic chains

Carlo Andrea Pagnacco<sup>1,2</sup>  | Xuban Gastearena<sup>1,3</sup>  |  
Estibaliz González de San Román<sup>4</sup>  | Jon M. Matxain<sup>1,3</sup>  |  
Fabienne Barroso-Bujans<sup>1,2,5</sup> 

<sup>1</sup>Donostia International Physics Center (DIPC), San Sebastian, Spain

<sup>2</sup>Centro de Física de Materiales, CSIC-UPV/EHU, San Sebastian, Spain

<sup>3</sup>Kimika Fakultatea, Euskal Herriko Unibertsitatea UPV/EHU, San Sebastian, Spain

<sup>4</sup>POLYMAT, University of the Basque Country UPV/EHU, Joxe Mari Korta Center, San Sebastian, Spain

<sup>5</sup>IKERBASQUE – Basque Foundation for Science, Bilbao, Spain

## Correspondence

Fabienne Barroso-Bujans, Donostia International Physics Center (DIPC), Paseo Manuel Lardizábal 4, 20018 Donostia– San Sebastian, Spain.  
Email: [fbarroso@dipc.org](mailto:fbarroso@dipc.org)

## Funding information

Ministerio de Ciencia, Innovación y Universidades, Grant/Award Number: PID2021-123438NB-I00; Basque Government, Grant/Award Numbers: IT1584-22, IT1566-22, PIBA 2021-1-0034

## Abstract

The synthesis of cyclic polymers via zwitterionic ring expansion polymerization is limited to a few number of monomer and catalyst pairs. Herein we report the synthesis of cyclic poly(*tert*-butyl glycidyl ether) through the polymerization of *tert*-butyl glycidyl ether (tBGE) with  $B(C_6F_5)_3$  in different reaction conditions that include different solvents, monomer to initiator ratio, monomer concentration and temperature. We found that bimodal molecular weight distribution is formed in almost all reaction conditions caused by cyclization of short chains. Subsequent chain elongation leads to the formation of cycles of higher molecular weight, particularly in cyclohexane and under bulk conditions. The formation of non-cyclic byproducts is common in all the systems investigated. Low molecular weight cyclic chains ( $M_n = 0.7$  kDa,  $\bar{D} = 1.1$ ) of high topological purity were successfully isolated by preparative gel permeation chromatography. By using a click scavenging protocol, the non-cyclic byproducts were eliminated from the high molecular weight fraction ( $M_n = 3$  kDa,  $\bar{D} = 1.3$ ) generating pure cyclic chains. Mechanistic investigation using density functional theory calculations was performed on the formation of zwitterionic intermediates and the transfer reaction to the monomer, which notably affects chain growth by the attack of the glycidyl oxygen of the monomer on the growing chain.

## KEYWORDS

$B(C_6F_5)_3$ , cyclic polymers, DFT calculations, Lewis acid, ring-opening polymerization

## 1 | INTRODUCTION

Cyclic polymers, also known as ring polymers, have gained significant interest in the field of polymer science and materials research due to their unique topology. This

topology imparts distinct properties and behavior to cyclic polymers compared to their linear analogues, offering exciting opportunities for studying their structure–function relationships.<sup>1–3</sup> In particular, water-soluble cyclic polymers are an important emerging area in

This is an open access article under the terms of the [Creative Commons Attribution](https://creativecommons.org/licenses/by/4.0/) License, which permits use, distribution and reproduction in any medium, provided the original work is properly cited.

© 2024 The Authors. *Journal of Polymer Science* published by Wiley Periodicals LLC.

biomedical research thanks to their proved higher chemical stability, prolonged blood circulation time and improved encapsulation efficiency compared to linear polymers.<sup>2,4-7</sup>

Zwitterionic ring expansion polymerization (ZREP) is a technique that allows the formation of cyclic polymers in one-pot reaction and large mass scales by making the right combination of monomer and catalyst.<sup>8-10</sup> For instance, N-heterocyclic carbenes were found to produce cyclic polyesters through a nucleophilic ZREP mechanism, whereas the  $B(C_6F_5)_3$  Lewis acid was found to generate cyclic polyethers through an electrophilic ZREP (eZREP) mechanism. The latter is based on the reaction of monosubstituted epoxides with  $B(C_6F_5)_3$ , which leads to the growth of macrozwitterionic propagating chains. The cyclic structure is maintained by electrostatic interactions that hold the chain ends together. At a certain reaction time, an end-to-end (end-biting) reaction occurs with the subsequent formation of cyclic chains and the expulsion of the catalyst from the growing chain. With this technique, cyclic polymers based on glycidyl phenyl ether, epichlorohydrine, benzyl glycidyl ether and 1,2-epoxytetradecane have been generated.<sup>8,9</sup> The reaction occurs either in solution or in bulk conditions with high monomer conversion. However, the polymer growth is limited by the expulsion of the catalyst, which reinitiates new polymer chains leading to polydisperse and low molecular weight products. The polymerization of glycidol with  $B(C_6F_5)_3$  occurs in a distinct manner due to the  $AB_2$  nature of the monomer, where both the epoxide and hydroxyl groups intervene in the polymerization.<sup>10-12</sup> Both, the active chain end and activated monomer mechanisms operate<sup>13</sup> to form hyperbranched polyglycidol, which is characterized by a cyclic core and branches as side chains.

Polymerization of protected glycidyl derivatives containing a protecting group for hydroxyl can be a convenient way to further produce cyclic polyglycidol (cPG) without branches. The most common protected glycidol derivatives are the ethoxyethyl glycidyl ether (EEGE), *tert*-butyl glycidyl ether (tBGE) and allyl glycidyl ether

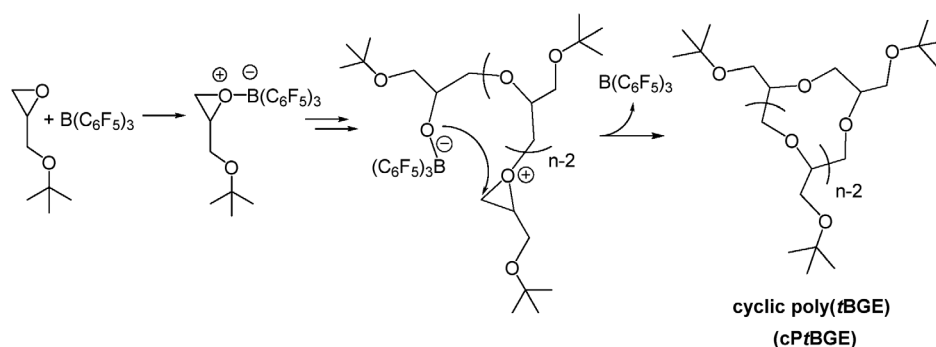
(AGE).<sup>14</sup> Our attempts to polymerize EEGE and AGE with  $B(C_6F_5)_3$  were unsuccessful in contrast to the polymerization of tBGE with  $B(C_6F_5)_3$  that does proceed, as demonstrated in this study.

Herein, we aim to study the polymerization of tBGE with  $B(C_6F_5)_3$  and evaluate the optimal conditions for the generation of cyclic structures of poly(tBGE). The mechanism of polymerization is depicted in Scheme 1, which is based on our previous studies on the eZREP of other monosubstituted epoxides with  $B(C_6F_5)_3$ .<sup>8-10</sup> We demonstrate that cyclic poly(tBGE) chains are formed in all the studied systems (different solvents, monomer to initiator concentration, monomer concentration and temperature) but that their formation is not under control. Chain transfer to monomer was found to play an important role in this polymerization due to the reactivity of glycidyl oxygen of tBGE, which is able to attack the epoxide ring in terminal active chains. Density functional theory (DFT) calculations were performed to support these reaction mechanisms. In addition, fractionation and click-scavenging protocols<sup>15</sup> were implemented to generate pure cyclic poly(tBGE) fractions.

## 2 | MATERIALS AND METHODS

### 2.1 | Materials

$B(C_6F_5)_3$ , *t*-butyl glycidyl ether (tBGE), dichloromethane (DCM), cyclohexane, dichloroethane (DCE), toluene, chloroform, sodium hydride (NaH), copper (I) bromide (CuBr), *N,N,N',N',N'*-pentamethyldiethylenetriamine (PDMETA), and sodium-L-(+) ascorbate were purchased from Sigma-Aldrich. tBGE was dried over  $CaH_2$ , degassed, distilled in vacuum at 70°C, and stored in Schlenk-flask under Ar atmosphere. Solvents were dried over  $CaH_2$ , degassed, distilled in vacuum at room temperature and stored in Schlenk-flask under Ar atmosphere.  $B(C_6F_5)_3$  was sublimated in vacuum at 110°C and stored in a glove-box under nitrogen atmosphere. Glove box and vacuum line were used to transfer all the chemicals in an inert atmosphere.



**SCHEME 1** eZREP of tBGE with  $B(C_6F_5)_3$ .

## 2.2 | Synthesis of poly(*t*-butyl glycidyl ether)

In a typical reaction in solution (Entry 5 of Table S1), 0.5 mL of tBGE (3.53 mmol) were introduced into a flame-dried round-bottom flask, dissolved in 3.0 mL of distilled toluene and stirred under an argon atmosphere. Then, 4.0 mg of  $B(C_6F_5)_3$  (7.86  $\mu$ mol) were dissolved in 1 mL of toluene and added to the monomer under magnetic stirring. The reaction was stirred for 96 h at 25°C. Then, the reaction was quenched by addition of 150  $\mu$ L of acetonitrile and passed through a column filled with basic  $Al_2O_3$ . The solvent was removed in a rotary evaporator and the polymer dried in a vacuum oven at 80°C.

In a typical reaction in solvent-free conditions (Entry 31 of Table S1), 0.5 mL of tBGE (3.53 mmol) were placed in a flame-dried round-bottom flask under an argon atmosphere and cooled to 0°C. Then, 4.0 mg of  $B(C_6F_5)_3$  (7.86  $\mu$ mol) were added to the monomer under magnetic stirring. The reaction was warmed up to 25°C and left for 24 h under stirring. Then, the reaction was quenched by addition of 150  $\mu$ L of acetonitrile, dissolved in about 5 mL of DCM and passed through a column filled with basic  $Al_2O_3$ . The solvent was removed in a rotary evaporator and the polymer dried in a vacuum oven at 80°C. The product was obtained as a transparent viscous paste. The monomer conversion of crude reactions was determined by  $^1H$ -NMR in  $CDCl_3$ .

## 2.3 | Kinetics

Monomer conversion and molecular weight were monitored as a function of time for the reaction of tBGE (1.5 mL, 11.0 mmol) with  $B(C_6F_5)_3$  (11.8 mg, 0.023 mmol) in 12.0 mL of toluene at 25°C. The reaction was sampled overtime by taking simultaneously two 0.1 mL aliquots of the reaction solution. One aliquot was added to 20  $\mu$ L of acetonitrile and then diluted in  $CDCl_3$ , and the other aliquot was added to 100  $\mu$ L of DMF + 0.1 LiBr (the eluent of gel permeation chromatography [GPC]).

Similarly, monomer conversion and molecular weight were monitored as a function of time for the reaction in solvent-free conditions. 1.5 mL of tBGE (11.0 mmol) were placed in a round-bottom flask at 0°C. Then 11.8 mg of  $B(C_6F_5)_3$  (0.023 mmol) were added to the monomer under magnetic stirring and the reaction was gradually warmed up to 25°C. The reaction was sampled continuously by taking 10 mg of sample aliquots with a spatula under a flux of argon. This was done twice. 20  $\mu$ L of acetonitrile were added to one of the samples and then diluted in  $CDCl_3$  for NMR analysis. The other 10 mg of

sample was dissolved with 100  $\mu$ L of DMF + 0.1 LiBr (the eluent of GPC).

## 2.4 | Fractionation

A poly(tBGE) sample was first synthesized by scaling up from 0.5 mL of tBGE to 12.5 mL under solvent-free conditions (reaction shown in Entry 31, Table S1). Then, the sample was separated in two fractions on a recycling preparative GPC, LaboAce LC-5060, from Japan Analytic Industry (JAI), equipped with a refractive index detector. Separation was performed at 30°C in 2,5HR and 3HR columns connected in series using the recycling mode. HPLC grade  $CHCl_3$  was used as a mobile phase at a rate of 10 mL/min. In a typical procedure 400 mg of poly(tBGE) were solubilized in 4 mL of  $CHCl_3$  and injected to the equipment. The fractions were manually collected. Low molecular weight impurities were removed from the sample. The solvent was removed in the rotary evaporator and the fractions dried in a vacuum oven at 80°C.

## 2.5 | Propargylation reaction

Low molecular weight (LMW) and high molecular weight (HMW) fractions of poly(tBGE) generated in the preparative GPC were subjected to a propargylation reaction. 10 mg of polymer were dissolved in 5 mL of dry THF. NaH (3.0 mg, 0.125 mmol) was added under a flux of Ar, and the mixture stirred for 30 min at 50°C. Propargyl bromide (80 wt% solution in toluene) (5.4 mg, 0.038 mol) was introduced dropwise to the reaction, and the mixture was stirred overnight at 50°C. Then, the solvent was evaporated in a rotary evaporator, the polymer dissolved in DCM, washed with distilled water ( $3 \times 10$  mL) and dried with sodium sulfate. The solvent was removed, and the polymer dried in a vacuum oven at 80°C.

## 2.6 | Synthesis of azide-functionalized amorphous silica gel

Azide-functionalized amorphous silica was synthesized following a procedure described in the literature<sup>16</sup> starting from amorphous silica gel (ASG) with a pore size of 60 Å, 200–425 mesh. Briefly, ASG (3.0 g) was dried in vacuum at 100°C overnight, then 22 mL of anhydrous toluene were added, and the suspension was sonicated for 30 min at 60°C. (3-bromopropyl)trichlorosilane (4.41 g, 17.2 mmol) was added dropwise and the suspension was stirred at 80°C overnight. After the reaction, the suspension was centrifuged and redispersed in toluene several times. The

product, a bromide-modified ASG, was dried in vacuum at 100°C. Then, a bromide-functionalized ASG was dispersed in 80 mL of DMF,  $\text{NaN}_3$  (1.0 g, 15.4 mmol) was added and the suspension was stirred at 80°C overnight. After the reaction, the suspension was redispersed in water and centrifuged several times. The product, an azide-functionalized ASG, was dried in vacuum at 100°C.

## 2.7 | Click scavenging

CuBr (1 g, 7.0 mmol) was suspended in 250 mL of glacial acetic acid under vigorous stirring for 24 h and then filtrated. This procedure was repeated three times. The precipitate was washed with dry ethanol and then with dry diethyl ether. CuBr (86 mg, 0.60 mmol), sodium-L-(+) ascorbate (119 mg, 0.60 mmol), PDMETA (125  $\mu\text{L}$ , 0.60 mmol) and azide-functionalized ASG (200 mg) were introduced in a round bottom flask (flame dried) and flushed with argon for 15 min. Then, 4 mL of distilled DCM were added and the mixture was suspended under vigorous stirring. The propargylated poly(tBGE) fraction of HMW (20 mg) was dissolved in 1 mL of DCM and dropwise added to the azide-functionalized ASG suspension. The mixture was stirred vigorously for 48 h at room temperature. The solid phase was filtrated and the filtrate washed with saturated solution of  $\text{NH}_4\text{Cl}$  until it turned clear. The organic layer was dried with  $\text{MgSO}_4$  and the solvent removed in a rotary evaporator. Yield = 54 wt%.

## 2.8 | Gel permeation chromatography

Gel permeation chromatography data were acquired using a Nexera instrument from Shimadzu using refractive index detector (RID-20A, Shimadzu). Separation was performed at 50°C by using a CTO 40C column oven and Polargel-M Guard  $50 \times 7.5 \text{ mm}^2$  and Polargel-M  $300 \times 7.5 \text{ mm}^2$ , 8  $\mu\text{m}$ , GPC columns. HPLC grade DMF containing 0.1% of LiBr with a flow of 1.0 mL/min was used as a mobile phase. The molecular weights of the polymers were determined by using polystyrene calibration curve and Lab Solutions 5.1 software from Shimadzu.

## 2.9 | Matrix assisted laser desorption index-time of flight mass spectrometry

MALDI-ToF MS measurements were performed on a Bruker Autoflex Speed system (Bruker, Germany) equipped with a Smartbeam-II laser (Nd:YAG, 355 nm, 2 kHz). Spectra were acquired in reflectron mode; each mass spectrum was the average of 10,000 shots. The laser

power was adjusted during the experiments. Poly(tBGE) samples were dissolved in THF at a concentration of 10 mg/mL. 2-[(2E)-3-(4-*tert*-butylphenyl)-2-methylprop-2-enylidene]malononitrile (DCTB) was used as a matrix coupled with sodium trifluoroacetate ( $\text{NaTFA}$ ) as cation donor.

## 2.10 | Nuclear magnetic resonance

Polymer samples were analyzed by  $^1\text{H}$  and  $^{13}\text{C}$  NMR. The spectra were recorded on a Bruker Avance Neo 500 at 25°C.  $\text{CDCl}_3$  was used as a solvent for tBGE and poly(tBGE) samples.

## 2.11 | Density functional theory calculations

Geometry optimization and vibrational frequency calculation were performed with DFT calculations<sup>17,18</sup> using Gaussian 16 program.<sup>19</sup> As in our previous study on the interactions between  $\text{B}(\text{C}_6\text{F}_5)_3$  and epoxide monomers,<sup>9,12</sup> TPSS exchange–correlation functional<sup>20</sup> and the DEF2TZVP basis set<sup>21,22</sup> were used and the empirical D3 version of Grimme's dispersion with the Becke–Johnson damping was considered.<sup>23</sup> Furthermore, environment effects ( $\epsilon = 4.7113$ ) were taken into account by means of the integral equation formalism of the polarized continuum model (IEFPCM).<sup>24</sup> The Harmonic vibrational frequencies were obtained for the optimized structures by the analytical differentiation of gradients, at the same level of theory of the geometry optimization, to identify whether the characterized structures were true minima. The zero-point vibrational energy (ZPVE) and the thermal ( $T = 298 \text{ K}$ ) vibrational corrections to the enthalpy were considered. Finally, these enthalpy values were used to calculate the adsorption enthalpies ( $\Delta H_{\text{ad}}$ ) of the different processes.

# 3 | RESULTS AND DISCUSSION

## 3.1 | Polymerization of tBGE

The polymerization of tBGE with  $\text{B}(\text{C}_6\text{F}_5)_3$  was performed by varying the monomer to initiator ratio ( $[\text{M}]_0/[\text{I}]_0$ ), monomer concentration ( $[\text{M}]_0$ ), solvent and temperature (Table S1). Figure 1A shows the GPC data of a series of samples synthesized in solvents of different polarity by keeping constant the rest of parameters,  $[\text{M}]_0/[\text{I}]_0 = 450$ ,  $[\text{M}]_0 = 0.8 \text{ M}$  and 25°C. Except in chloroform, a bimodal molecular weight distribution was observed by exhibiting a LMW peak with a molecular

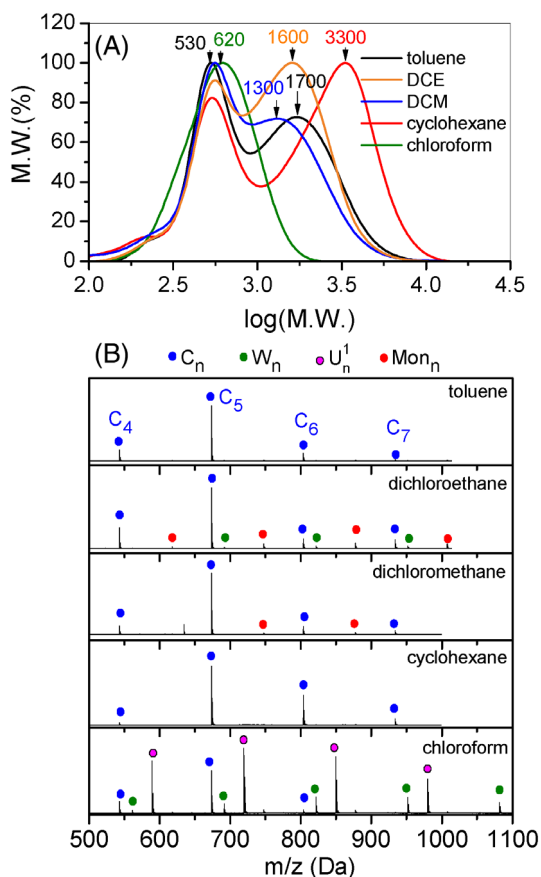
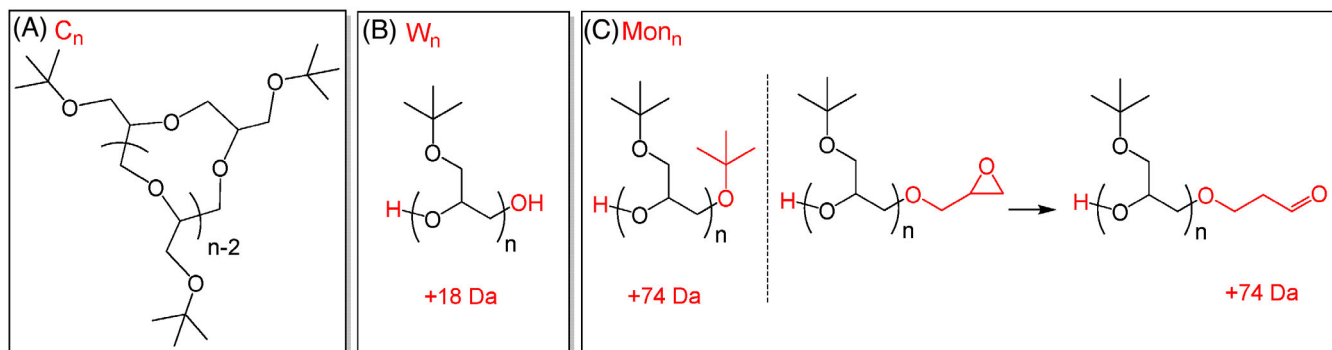


**FIGURE 1** (A) Gel permeation chromatography (GPC) (with PS calibration curve,  $M_p$  values indicated) and (B) MALDI-ToF MS (+Na<sup>+</sup>) data of poly(tBGE) synthesized in different solvents at 25°C.  $[M]_0/[I]_0 = 450$ ,  $[M]_0 = 0.8$  M. Entries 5, 14, 17, 18 and 24 of Table S1.  $C_n$  indicates cyclic chains where  $M_{obs}(C_n) = nM_{tBGE} + M_{Na}$ .  $W_n$ ,  $U_n^1$  and  $Mon_n$  species appear at a peak position +18, +46 and +74 Da from those of  $C_n$ , respectively.

weight at the peak position ( $M_p$ ) of 530 g/mol. The HMW peak exhibited a slight dependence with the solvent polarity, in which  $M_p$  changed from 1300 to 3300 g/mol from more to less polar [dielectric constant,  $\epsilon$ : DCE (10.42) > DCM (8.93) > toluene (2.38) > cyclohexane (2.02)]. The polymerization performed in cyclohexane was the one exhibiting the highest HMW/LMW peak intensity ratio, which is in line with the highest molecular weight achieved in this series of samples. MALDI-ToF MS was used to analyze the chain composition in both molecular weight regions. To avoid ion suppression of higher masses, both molecular weight ranges, LMW and HMW, were analyzed separately. By analyzing the mass spectra of poly(tBGE) in the LMW region, a peak distribution corresponding to  $M_{obs}(C_n; Da) = nM_{tBGE} + M_{Na}$  of sodium-complexed chains were detected in all cases (see the isotopic distribution in Figure S1). These species are attributed to the formation of cyclic poly(tBGE) chains

(Scheme 2A). In chloroform, the spectrum is dominated by the peaks at  $M_{obs}(U_n^1; Da) = nM_{tBGE} + M_{Na} + 46.05$  and  $M_{obs}(W_n; Da) = nM_{tBGE} + M_{Na} + 18.02$ .  $W_n$  are attributed to linear poly(tBGE) chains terminated in two hydroxyl groups (Scheme 2B).  $W_n$  species are likely formed by initiation with a protic acid and/or transfer with adventitious water, as it has been described in the polymerization of other epoxide monomers.<sup>8,9</sup>  $U_n^1$  are unknown species. However, they could have formed through the reaction of active chains with the ethanol used as a stabilizer for chloroform. In solvents of higher polarity, such as DCE and DCM, other species with lower peak intensity were detected corresponding to  $M_{obs}(Mon_n; Da) = nM_{tBGE} + M_{Na} + 74.06$ . These species are attributed to linear poly(tBGE) chains terminated in a hydroxyl, and a *tert*-butoxy or a methoxy oxirane group (Scheme 2C), which are formed by transfer reaction to monomer. Both end groups have identical masses and are not distinguishable by MALDI. However, the appearance of oxypropanal end-group signals in the <sup>1</sup>H NMR spectrum (Figure S2) and a C=O aldehyde signal at 202.0 ppm (Figure S3) supports the formation of chains ended in methoxy oxirane groups that were transformed into aldehydes via Meinwald rearrangement.<sup>25,26</sup> The formation of *tert*-butoxy end groups is mechanistically less probable, as discussed below.

In the HMW range of MALDI-ToF MS data, the cyclic  $C_n$  species were only detected in cyclohexane suggesting that non-polar media favor cyclization (Figure 2). However, the formation of cycles was not observed in toluene, even when this solvent presents a low  $\epsilon$  as cyclohexane suggesting that other unidentified factors play a role in the cyclization. In all the solvents, the formation of  $Mon_n$  and  $W_n$  species was detected, which are probably the responsible for the limited chain growth and therefore for the low molecular weights of the obtained products. A study of the effects of  $[M]_0/[I]_0$  and  $[M]_0$  on the chain growth in toluene resulted in similar GPC traces indicating that the chain growth is totally independent of such factors (Figure 3A). MALDI-ToF MS analysis in the LMW region of samples obtained at different  $[M]_0/[I]_0$  exhibited peak distributions corresponding to only  $C_n$  specimens confirming the formation of cyclic chains in those conditions (Figure 4A). In the HMW region, however, the cyclic species were not detected, but only the  $Mon_n$  and  $W_n$  specimens (Figure 4B). By decreasing the temperature to 10°C, the reaction became too slow reaching only 33 mol% of conversion in 144 h. By raising the temperature to 50°C, the monomer conversion went to 100% in only 24 h, which is much faster than 96 h at 25°C (Figure 3B). With increasing temperature, the HMW peak showed a relative increase compared to the LMW peak, but the formation of cycles were only



**SCHEME 2** Structures assigned to MALDI-ToF MS signals observed in Figure 1 and the corresponding mass shift values from  $C_n$  signal.

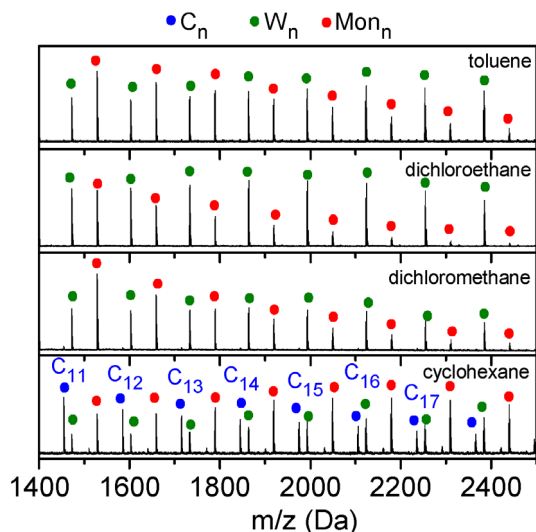


**FIGURE 2** MALDI-ToF MS ( $+Na^+$ ) data of poly(tBGE) synthesized in different solvents at  $25^\circ C$ .  $[M]_0/[I]_0 = 450$ ,  $[M]_0 = 0.8$  M. Entries 5, 14, 17, 18 and 24 of Table S1.  $C_n$  indicates cyclic chains where  $M_{obs}(C_n) = nM_{tBGE} + M_{Na}$ .  $W_n$ , and  $Mon_n$  species appear at a peak position  $+18$  and  $+74$  Da from those of  $C_n$ , respectively.

observed in the LMW peak (Figure 5A). Instead, the HMW peak showed the presence of  $Mon_n$  and  $W_n$  specimens, the latter with higher relative intensity at  $50^\circ C$  (Figure 5B). Further study of the effects of  $[M]_0/[I]_0$  and  $[M]_0$  on the chain growth in other solvents, dichloromethane and cyclohexane, exhibited similar GPC traces (Figures S4 and S5) with some exceptions likely related with the non-completion of the reaction (i.e., 57% monomer conversion in DCM using  $[M]_0 = 0.4$  M and  $[M]_0/[I]_0 = 820$ , Table S1).

To gain further insight into the polymerization of tBGE with  $B(C_6F_5)_3$ , the reaction was performed in solvent-free conditions. At  $25^\circ C$  the polymerization occurred too fast showing a high exothermicity. At  $0^\circ C$  the polymerization did not proceed for 3 days. However,

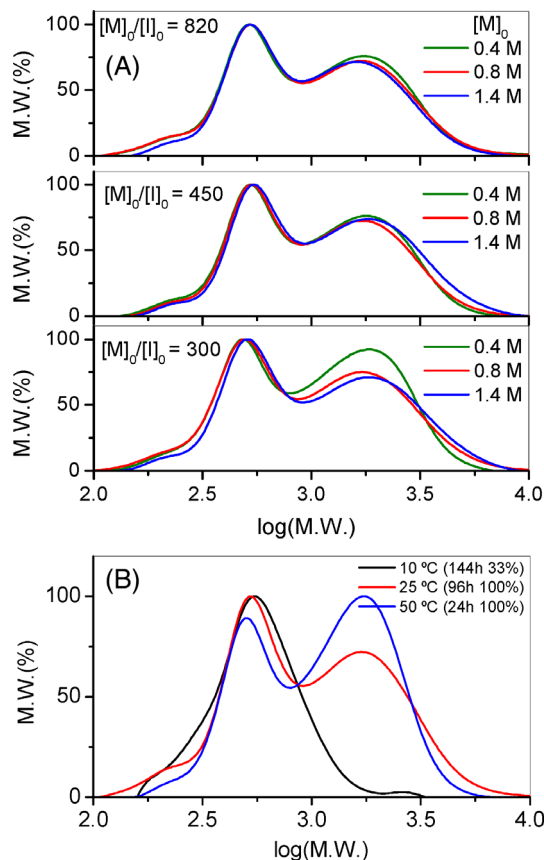


**FIGURE 3** Gel permeation chromatography (GPC) traces of poly(tBGE) synthesized in toluene (A) at different  $[M]_0$  and  $[M]_0/[I]_0$  at  $25^\circ C$  (Entries 1–9 of Table S1); and (B) at different temperatures by keeping constant  $[M]_0/[I]_0 = 820$  and  $[M]_0 = 0.8$  M (Entries 5, 10 and 11 of Table S1).

the polymerization occurred without violence by adding the initiator at  $0^\circ C$  and subsequently increasing the temperature to  $25^\circ C$ . By increasing the  $[M]_0/[I]_0$  ratio from 300 to 820, the HMW peak shifted to higher mass values while the LMW peak remained at the same position (Figure 6). MALDI-ToF MS analysis in the LMW region exhibited peak distributions corresponding to  $C_n$

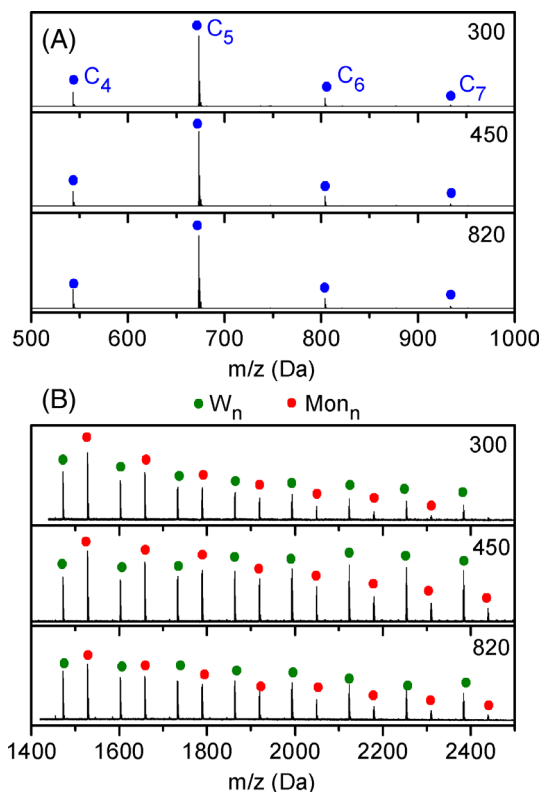


**FIGURE 4** MALDI-ToF-MS (+Na<sup>+</sup>) of poly(tBGE) synthesized in toluene at different  $[M]_0/[I]_0 = 300, 450$  and  $820$ .  $[M]_0 = 0.8$  M at  $25^\circ\text{C}$ . Entries 2, 5 and 8 of Table S1. Analysis in the (A) low molecular weight (LMW) and (B) higher molecular weight (HMW) region.

specimens, and at lower  $[M]_0/[I]_0$  values,  $\text{Mon}_n$  and  $W_n$  species appear (Figure 7A). In the HMW, the peak analysis exhibited the formation of a number of different species, including unidentified chains,  $U^2_n$ ,  $U^3_n$  and  $U^4_n$ , at  $[M]_0/[I]_0 = 300$ , which vanished with the increase of  $[M]_0/[I]_0$  to  $820$  (Figure 7B). These results clearly indicate that the number of transfer reactions increase with the amount of  $\text{B}(\text{C}_6\text{F}_5)_3$  in the bulk media, where there is a larger number of shorter active growing chains that might conduct to transfer reactions. On the contrary, by decreasing the amount of  $\text{B}(\text{C}_6\text{F}_5)_3$ , larger active chains are formed which terminate by end-to-end cyclization rather than by transfer.

### 3.2 | Kinetics

The polymerization in toluene showed that LMW species are mainly formed during the first 7.5 h of reaction after which the HMW peak intensity start increasing (Figure 8). The peak intensity ratio of HMW and LMW peaks ( $I_{\text{HMW}}/I_{\text{LMW}}$ ) reached a plateau in about 24 h. At this reaction time, the monomer conversion was only of 64 mol%, a

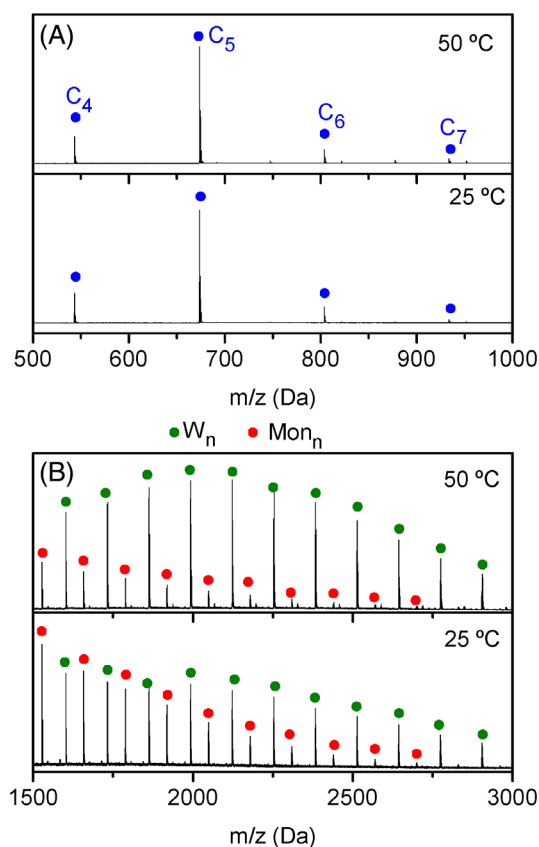


**FIGURE 5** MALDI-ToF MS (+Na<sup>+</sup>) data of poly(tBGE) synthesized in toluene at  $25$  and  $50^\circ\text{C}$ .  $[M]_0/[I]_0 = 450$ ,  $[M]_0 = 0.8$  M. Entries 5 and 11 of Table S1. Analysis in the (A) low molecular weight (LMW) and (B) higher molecular weight (HMW) region.

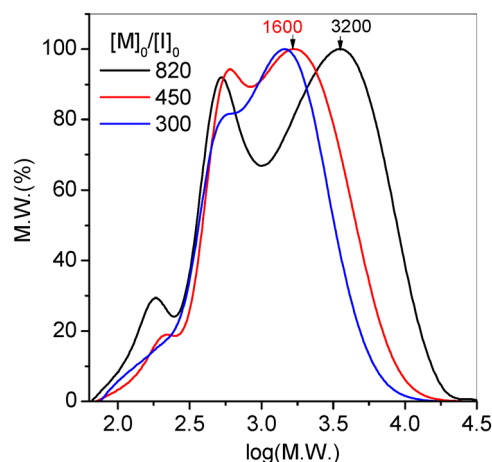


**FIGURE 6** Gel permeation chromatography (GPC) (with PS calibration curve,  $M_p$  values indicated) of crude samples of poly(tBGE) synthesized in solvent-free conditions at different  $[M]_0/[I]_0$  at  $25^\circ\text{C}$ . Entries 29–31 of Table S1.

value that increases to 77 mol% at 144 h. This slow reaction rate does not favor chain growth, causing free monomer to produce transfer reactions leading to the formation of

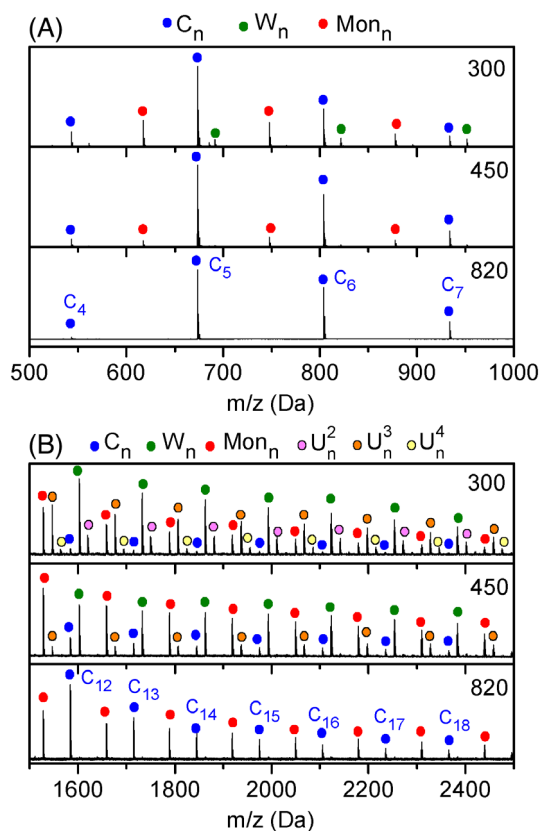


**FIGURE 7** MALDI-ToF MS data of poly(tBGE) synthesized in solvent-free conditions at different  $[M]_0/[I]_0 = 300, 450$  and  $820$  at  $25^\circ\text{C}$ . Entries 29–31 of Table S1. Analysis in the (A) low molecular weight (LMW) and (B) higher molecular weight (HMW) region.  $C_n$  indicates cyclic chains where  $M_{\text{obs}}(C_n) = nM_{\text{tBGE}} + M_{\text{Na}}$ .  $W_n$ , and  $\text{Mon}_n$  species appear at a peak position  $+18$  and  $+74$  Da from those of  $C_n$ , respectively.  $U_n^2$ ,  $U_n^3$  and  $U_n^4$  are unknown species appearing at  $+36$ ,  $+92$  and  $+110$  Da from those of  $C_n$ , respectively.

$\text{Mon}_n$  species. In contrast to solution polymerization, the polymerization under solvent-free conditions was very fast. The catalyst had to be added at  $0^\circ\text{C}$ , because when it was added at  $25^\circ\text{C}$  the reaction occurred in a violent manner. Then, the reaction was carefully warmed up to  $25^\circ\text{C}$ . The first data point was taken at 20 min after temperature stabilization at  $25^\circ\text{C}$ . Monitoring of the reaction showed that it was almost complete in 1 h by reaching 98% of monomer conversion (Figure 9). At 20 min of reaction, LMW species predominated, and after only 40 min, the amounts of HMW species exceeded those of LMW indicating a rapid chain growth. After 1 h there was no significant change in the molecular weight as a result of reaction completion. However, we monitored the reaction for up to 30 h to determine whether or not chain fusion events occurred, as observed in the bulk polymerization of glycidol with  $\text{B}(\text{C}_6\text{F}_5)_3$ .<sup>10</sup> The results indicate that such events do not occur in the current polymerization probably because

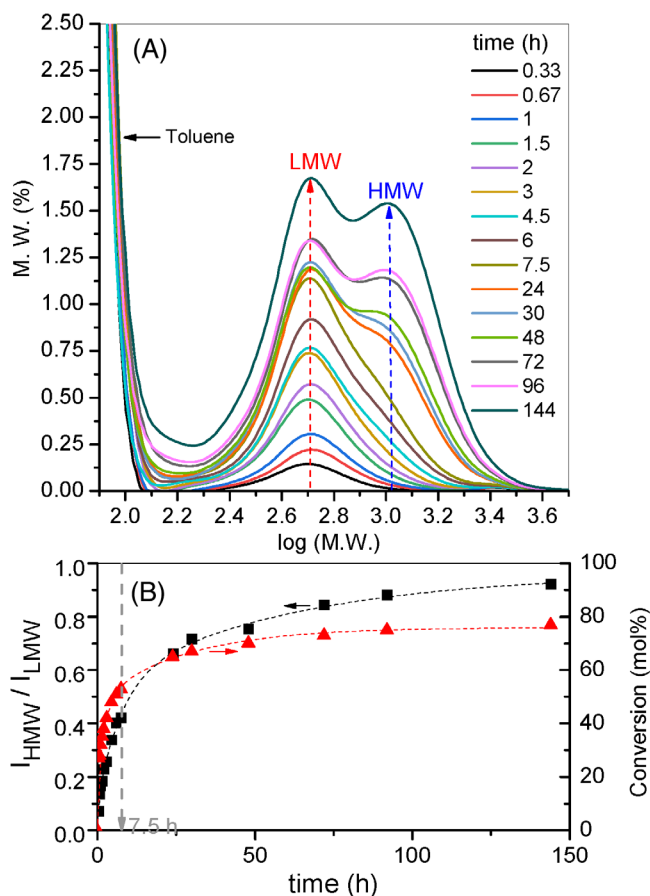


**FIGURE 8** (A) Gel permeation chromatography (GPC) monitoring (with PS calibration curve) of tBGE polymerization in toluene at  $25^\circ\text{C}$ .  $[M]_0/[I]_0 = 450$ ,  $[M]_0 = 0.8$  M. (B) Peak intensity ratio of higher molecular weight (HMW) and low molecular weight (LMW) peaks ( $I_{\text{HMW}}/I_{\text{LMW}}$ ) and monomer conversion.

the zwitterionic growing chains are quickly deactivated either by end biting or transfer reactions.

### 3.3 | Purification of the cycles

To verify the cyclic content in the samples, a poly(tBGE) product synthesized in bulk with a  $[M]_0/[I]_0$  of 800 was fractionated in two fractions of LMW ( $M_n = 0.7$  kDa,  $\bar{D} = 1.1$ ) and HMW ( $M_n = 3$  kDa,  $\bar{D} = 1.3$ ) in a preparative GPC (Figure S6). Both fractions were reacted with progargyl bromide by following previous work<sup>15</sup> and the products analyzed by MALDI-ToF MS (Figure 10). The LMW fraction exhibited no signal shift after reaction demonstrating the absence of hydroxyl-terminated chains and confirming the cyclic purity in this fraction. Instead, the HMW fraction exhibited mass shifts of  $+38$  Da corresponding to the addition of one progargyl bromide unit from the peaks corresponding to  $C_n$  and  $\text{Mon}_n$  species and a mass shift of  $+76$  Da corresponding to the addition



of two propargyl bromide units from the peaks corresponding to  $W_n$  specimens. End group functionalization with one propargyl bromide unit confirmed the presence of mono-hydroxyl terminated chains in  $Mon_n$  as well as the presence of isomeric tadpole chains ( $TP_n$ ) with identical mass as that of  $C_n$ . The mechanism for the formation of tadpole structures has been discussed elsewhere.<sup>15,27</sup>

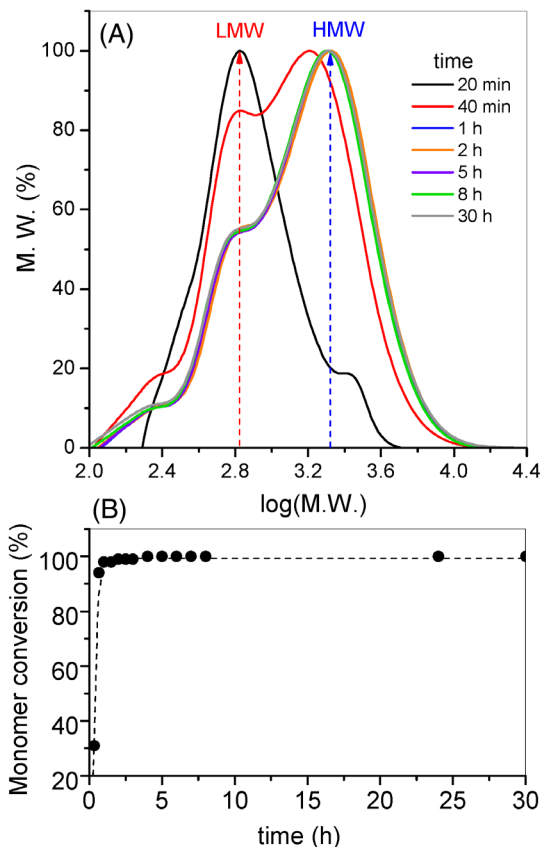


**FIGURE 9** (A) Gel permeation chromatography (GPC) monitoring (with PS calibration curve) of tBGE polymerization in bulk at 25°C (the catalyst was added at 0°C).  $[M]_0/[I]_0 = 450$ . (B) Monomer conversion.

End group functionalization with two propargyl bromides confirmed the di-hydroxyl terminated structure of  $W_n$  specimens ( $^1H$ – $^{13}C$  HSQC NMR spectrum is shown in Figure S7).

The HMW fraction was subjected to a topological purification by click-scavenging.<sup>15</sup> This consists in reacting the hydroxyl groups of non-cyclic impurities with propargyl bromide, as shown in Figure 10, and then reacting the propargylated chains with an azide-modified silica using Cu(I) catalyst via Cu-catalyzed azide–alkyne cycloaddition (CuAAC) click reaction. Upon filtration, only the cyclic chains should be obtained. MALDI-ToF MS data of a HMW sample subjected to this protocol is shown in Figure 11. As observed, the peaks corresponding to  $TP_n$ ,  $W_n$ , and  $Mon_n$  were no longer detected and only a distribution of mass peaks corresponding to only  $C_n$  specimens was observed.

### 3.4 | Density functional theory calculations

Density functional theory calculations of the reaction between tBGE and  $B(C_6F_5)_3$  exhibited the energy profile

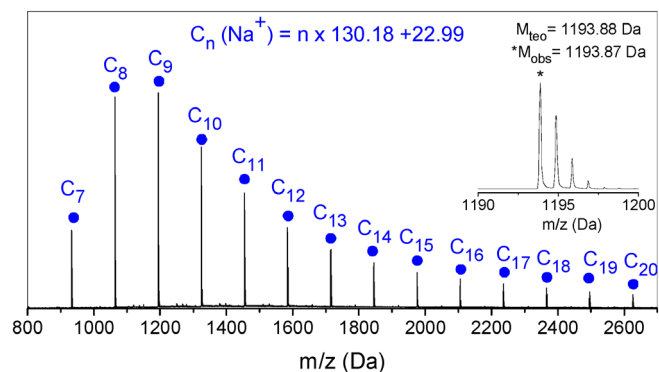


**FIGURE 11** MALDI-ToF-MS (+ $Na^+$ ) of higher molecular weight (HMW) fraction purified by click-scavenging.<sup>15</sup>

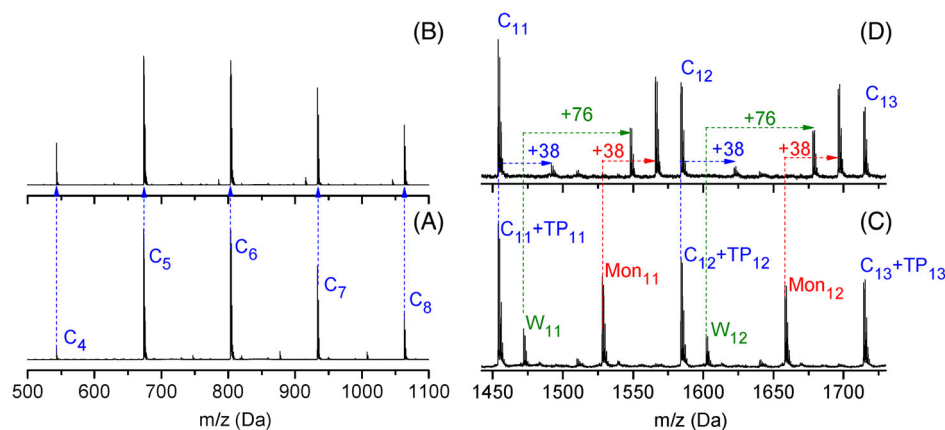


**FIGURE 10** MALDI-ToF-MS (+ $Na^+$ ) of (A) low molecular weight (LMW) fraction of poly(tBGE) generated in bulk and (B) the reacted LMW fraction with propargyl bromide. (C) higher molecular weight (HMW) fraction of poly(tBGE) generated in bulk and (D) the reacted HMW fraction with propargyl bromide.

**FIGURE 12** Enthalpy profiles of the reaction between tBGE and  $B(C_6F_5)_3$  at 298 K.  $I^{AC}$  is the activated complex at the initiation step.  $P_1^{INTa}$  is the adsorption step of a second tBGE molecule at the alpha carbon of epoxide,  $P_1^{TS}$  is the transition state and  $P_1^{INTb}$  is the final product of the first step of propagation. The profile corresponding to the attack from epoxide is depicted in blue and that from glycidyl oxygen in orange. Finally, the orange  $P_1^{INTb}$  product can undergo cleave producing the products  $P_1^c$ .

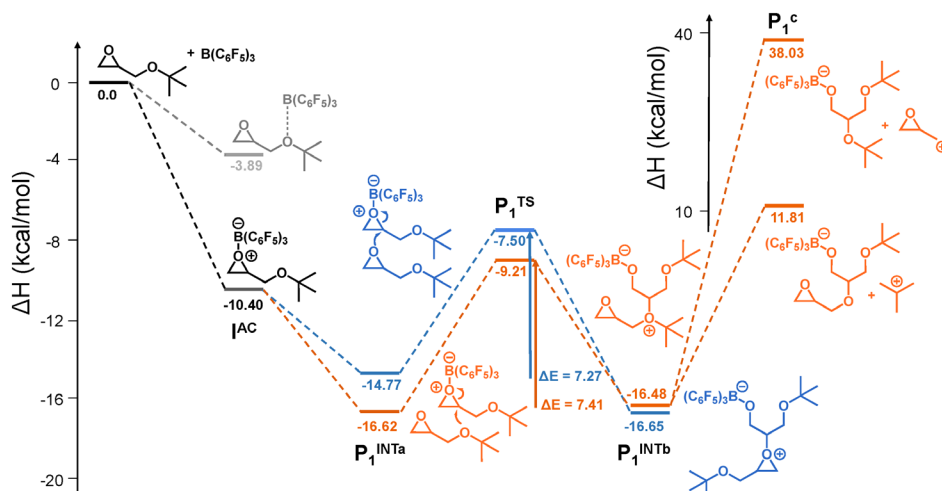
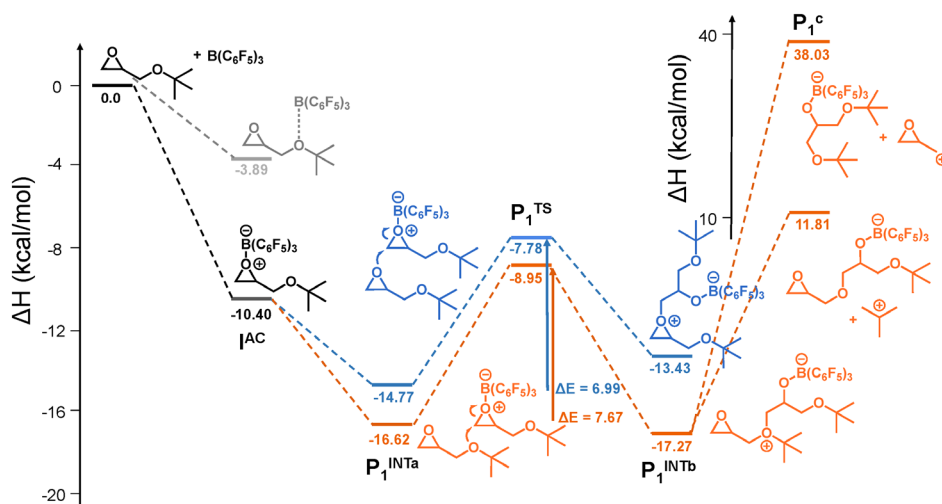


**FIGURE 13** Enthalpy profiles of the reaction between tBGE and  $B(C_6F_5)_3$  at 298 K.  $I^{AC}$  is the activated complex at the initiation step.  $P_1^{INTa}$  is the adsorption step of a second tBGE molecule at the beta carbon of epoxide,  $P_1^{TS}$  is the transition state and  $P_1^{INTb}$  is the final product of the first step of propagation. The profile corresponding to the attack from epoxide is depicted in blue and that from glycidyl oxygen in orange. Finally, the orange  $P_1^{INTb}$  product can undergo cleave producing the products  $P_1^c$ .



shown in Figures 12 and 13.  $B(C_6F_5)_3$  showed a strong interaction with tBGE epoxide with an adsorption enthalpy of  $-10.40$  kcal/mol and O–B distance of  $1.6$  Å (activated complex at initiation,  $I^{AC}$ ), which is in agreement with the previous calculations based on epoxide monomers and  $B(C_6F_5)_3$ .<sup>9,12</sup> The interaction with glycidyl ether oxygen also exhibited a negative enthalpy of  $-3.89$  kcal/mol but with a much longer O–B distance of  $3.97$  Å. The formation of the last complex is therefore less likely. Then, the calculation of the adsorption energies of a second monomer to the methine ( $\alpha$ ) and methylene ( $\beta$ ) carbons of activated tBGE monomer ( $P_1^{INTa}$ ) showed negative enthalpies indicating stabilization. Interestingly, the monomer adsorption from the glycidyl oxygen (in orange) is even more stable than that occurring from the epoxide oxygen (in blue). Then, the next step leads to the formation of products ( $P_1^{INTb}$ ) with negative enthalpies or close to zero, as well as low  $\Delta E$  values in the range of  $7$  kcal/mol, indicating that both attacks are likely. The differences in the attack on the  $\alpha$  and  $\beta$  carbons are very subtle, which suggest that both

carbons are prone to be attacked. The attack from epoxide oxygen will conduct to a propagating oxonium ion (in blue) but the attack from glycidyl ether oxygen will conduct to an ionic non-polymerizable chain (in orange) that can undergo excision of *tert*-butyl or methyloxirane carbocations to form the  $Mon_n$  chains shown in Scheme 2C. The high energy required to undergo the excision of both groups is related to the strong covalent character of the C–O bond that must be broken and the instability of the leaving carbocations (*tert*-butyl or methyloxirane). The C–O distance for O-*tert*-butyl is  $1.62$  and  $1.48$ – $1.49$  Å for O-methyloxirane, which correspond to very stable bonds. Therefore a high energy is needed to break them. Nevertheless, the O-*tert*-butyl bond is notoriously weaker than O-methyloxirane bond, which would explain the lower enthalpy found for the release of a *tert*-butyl carbocation. This, together with the higher stability of the *tert*-butyl carbocation (better leaving group) supports the formation of methoxy oxirane end groups (Scheme 2C, right) as a collateral reaction.

### 3.5 | Final remarks on the polymerization of tBGE with B(C<sub>6</sub>F<sub>5</sub>)<sub>3</sub>

The characteristic features of the eZREP of tBGE with B(C<sub>6</sub>F<sub>5</sub>)<sub>3</sub> can be summarized as follows. The LMW component primarily consists of cyclic oligomeric chains in most of the evaluated systems. Their formation at the early stages of polymerization points to a system dominated by end-to-end cyclization, as it occurs in many cationic ring opening polymerization systems.<sup>28</sup> Cyclization competes with propagation by establishing kinetic and thermodynamic equilibria, which seem not to depend on the initial monomer concentration, monomer to initiator ratio, nor temperature in the solution polymerization. The cyclic content in the HMW fraction is lower than in the LMW fraction due to the occurrence of termination reactions other than end-to-end cyclization. Clearly, for longer chains, the probability of both ends meeting becomes negligible, and random back-biting involving the reaction from oxygens along the main chain with terminal active species becomes more frequent. This type of termination would lead to the formation of tadpole structures, as detected in the HMW region.

Termination by transfer to monomer leading to Mon<sub>n</sub> specimens occurs in all the systems investigated. According to DFT calculations, the attack of glycidyl oxygen on the growing chain is an energetically and kinetically competing process with propagation. This would explain why the transfer reaction to monomer cannot be eliminated in this polymerization system under any of the reaction conditions investigated.

MALDI-ToF-MS is a valuable tool for examining chain composition, but quantification of cyclic species cannot be done with precision because the ionization of distinct species can be different. The detection of only cyclic species in the LMW region together with their detection in the HMW region, despite being accompanied by non-cyclic species, was the criterion used to determine whether a system favored or did not favor cyclization. Following this criterion, we can say that bulk polymerization and polymerization in cyclohexane are the ones that provides the largest amounts of cyclic components. The LMW region, which contains the largest amounts of pure cyclic component, represents 20% of the total GPC chromatogram for the bulk polymerization and 30% for the polymerization in cyclohexane. End-biting cyclization is clearly favored when both chain ends containing negative and positive charges are held together. It is likely that ionic interactions between oppositely charged chain ends are favored by the high viscosity and low chain mobility of bulk polymerization. Similarly, a low dissociation of ion pairs in cyclohexane would explain these results.

## 4 | CONCLUSIONS

The polymerization of *tert*-butyl glycidyl ether with B(C<sub>6</sub>F<sub>5</sub>)<sub>3</sub> conducts to the formation of cyclic poly(*tert*-butyl glycidyl ether) chains and non-cyclic specimens. Fractionation and purification protocols were successfully implemented to generate pure cyclic chains. DFT calculations supported the formation of zwitterionic intermediates in an eZREP mechanism and the formation of linear impurities provided by transfer reactions to monomer. These findings underscore the complexity of the polymerization process and highlight avenues for further research aimed at elucidating and controlling the synthesis of cyclic polymers with tailored properties.

### ACKNOWLEDGMENTS

We gratefully acknowledge support from MCIN/AEI/10.13039/501100011033 and by “ERDF A way of making Europe” (PID2021-123438NB-I00), and Basque Government (IT1584-22, IT1566-22 and PIBA 2021-1-0034). Xuban Gastearena thanks the Basque Government for funding through the Fellowship Number PRE\_2022\_1\_0235.


### CONFLICT OF INTEREST STATEMENT

The authors declare no conflicts of interest.

### ORCID

Carlo Andrea Pagnacco  <https://orcid.org/0000-0001-8088-3613>

Xuban Gastearena  <https://orcid.org/0009-0004-5262-2853>

Estibaliz González de San Román  <https://orcid.org/0000-0001-5440-2695>

Jon M. Matxain  <https://orcid.org/0000-0002-6342-0649>

Fabienne Barroso-Bujans  <https://orcid.org/0000-0002-9591-5646>

### REFERENCES

- [1] J. Ochs, C. A. Pagnacco, F. Barroso-Bujans, *Prog. Polym. Sci.* **2022**, *134*, 101606.
- [2] F. M. Haque, S. M. Grayson, *Nat. Chem.* **2020**, *12*, 433.
- [3] M. Kruteva, J. Allgaier, D. Richter, *Macromolecules* **2023**, *56*, 7203.
- [4] N. Nasongkla, B. Chen, N. Macaraeg, M. E. Fox, J. M. J. Fréchet, F. C. Szoka, *J. Am. Chem. Soc.* **2009**, *131*, 3842.
- [5] B. Chen, K. Jerger, J. M. J. Fréchet, F. C. Szoka Jr., *J. Control. Release* **2009**, *140*, 203.
- [6] B. Zhang, H. Zhang, Y. Li, J. N. Hoskins, S. M. Grayson, *ACS Macro Lett.* **2013**, *2*, 845.
- [7] R. Liénard, J. De Winter, O. Coulembier, *J. Polym. Sci.* **2020**, *58*, 1481.
- [8] I. Asenjo-Sanz, A. Veloso, J. I. Miranda, J. A. Pomposo, F. Barroso-Bujans, *Polym. Chem.* **2014**, *5*, 6905.
- [9] F. M. Haque, C. M. Schexnayder, J. M. Matxain, F. Barroso-Bujans, S. M. Grayson, *Macromolecules* **2019**, *52*, 6369.

- [10] M. A. Al Assiri, E. Gómez Urreiziti, C. A. Pagnacco, E. G. de San Román, F. Barroso-Bujans, *Eur. Polym. J.* **2022**, *171*, 111194.
- [11] S. E. Kim, H. J. Yang, S. Choi, E. Hwang, M. Kim, H.-J. Paik, J.-E. Jeong, Y. I. Park, J. C. Kim, B.-S. Kim, S.-H. Lee, *Green Chem.* **2022**, *24*, 251.
- [12] E. Gómez Urreiziti, X. Gastearena, A. Lam, E. G. de San Román, J. I. Miranda, J. M. Matxain, F. Barroso-Bujans, *Mater. Today Chem.* **2024**, *37*, 101993.
- [13] S. Penczek, J. Pretula, *ACS Macro Lett.* **2021**, *10*, 1377.
- [14] P. Pouyan, M. Cherri, R. Haag, *Polymers* **2022**, *14*, 2684.
- [15] F. M. Haque, A. Alegría, S. M. Grayson, F. Barroso-Bujans, *Macromolecules* **1870**, 2017, 50.
- [16] R. Ranjan, W. J. Brittain, *Macromolecules* **2007**, *40*, 6217.
- [17] W. Kohn, L. J. Sham, *Phys. Rev.* **1965**, *140*, A1133.
- [18] P. Hohenberg, W. Kohn, *Phys. Rev.* **1964**, *136*, B864.
- [19] M. J. Frisch, G. W. Trucks, H. B. Schlegel, G. E. Scuseria, M. A. Robb, J. R. Cheeseman, G. Scalmani, V. Barone, G. A. Petersson, H. Nakatsuji, X. Li, M. Caricato, A. V. Marenich, J. Bloino, B. G. Janesko, R. Gomperts, B. Mennucci, H. P. Hratchian, J. V. Ortiz, A. F. Izmaylov, J. L. Sonnenberg, F. D. Williams, F. Lipparini, F. Egidi, J. Goings, B. Peng, A. Petrone, T. Henderson, D. Ranasinghe, V. G. Zakrzewski, J. Gao, N. Rega, G. Zheng, W. Liang, M. Hada, M. Ehara, K. Toyota, R. Fukuda, J. Hasegawa, M. Ishida, T. Nakajima, Y. Honda, O. Kitao, H. Nakai, T. Vreven, K. Throssell, J. A. Montgomery Jr., J. E. Peralta, F. Ogliaro, M. J. Bearpark, J. J. Heyd, E. N. Brothers, K. N. Kudin, V. N. Staroverov, T. A. Keith, R. Kobayashi, J. Normand, K. Raghavachari, A. P. Rendell, J. C. Burant, S. S. Iyengar, J. Tomasi, M. Cossi, J. M. Millam, M. Klene, C. Adamo, R. Cammi, J. W. Ochterski, R. L. Martin, K. Morokuma, O. Farkas, J. B. Foresman, D. J. Fox, Gaussian 16 Rev. C.01, Wallingford, CT. **2016**.
- [20] J. Tao, J. P. Perdew, V. N. Staroverov, G. E. Scuseria, *Phys. Rev. Lett.* **2003**, *91*, 146401.
- [21] F. Weigend, R. Ahlrichs, *Phys. Chem. Chem. Phys.* **2005**, *7*, 3297.
- [22] F. Weigend, *Phys. Chem. Chem. Phys.* **2006**, *8*, 1057.
- [23] S. Grimme, S. Ehrlich, L. Goerigk, *J. Comput. Chem.* **2011**, *32*, 1456.
- [24] G. Scalmani, M. J. Frisch, *J. Chem. Phys.* **2010**, *132*, 114110.
- [25] C. Xu, J. Xu, *Org. Biomol. Chem.* **2020**, *18*, 127.
- [26] J. Meinwald, S. S. Labana, M. S. Chadha, *J. Am. Chem. Soc.* **1963**, *85*, 582.
- [27] J. M. O'Neill, J. Mao, F. M. Haque, F. Barroso-Bujans, S. M. Grayson, C. Wesdemiotis, *Analyst* **2022**, *147*, 2089.
- [28] K. Matyjaszewski, *Cationic Polymerizations: Mechanisms, Synthesis & Applications*, Marcel Dekker, Inc., New York **1996**.

## SUPPORTING INFORMATION

Additional supporting information can be found online in the Supporting Information section at the end of this article.

**How to cite this article:** C. A. Pagnacco, X. Gastearena, E. González de San Román, J. M. Matxain, F. Barroso-Bujans, *J. Polym. Sci.* **2024**, *62*(12), 2704. <https://doi.org/10.1002/pol.20240112>